NASA Technical Memorandum 102518
AIAA-90-0600

Comparison of 3-D Viscous Flow Computations of Mach 5 Inlet With Experimental Data

D.R. Reddy
Sverdrup Technology, Inc.
NASA Lewis Research Center Group
Cleveland, Ohio

and

T.J. Benson and L.J. Weir
National Aeronautics and Space Administration
Lewis Research Center
Cleveland, Ohio

Prepared for the
28th Aerospace Sciences Meeting
sponsored by the American Society of Aeronautics and Astronautics
Reno, Nevada, January 8-11, 1990

NASA

COMPARISON OF 3-D VISCOUS FLOW COMPUTATIONS OF MACH 5 INLET WITH EXPERIMENTAL DATA

D.R. Reddy*
Sverdrup Technology, Inc.
NASA Lewis Research Center Group
Cleveland, Ohio 44135

T.J. Benson** and L.J. Weir***
NASA Lewis Research Center
Cleveland, Ohio 44135

Abstract

A time marching 3-D full Navier-Stokes code, called PARC3D, is validated for an experimental Mach 5 inlet configuration using the data obtained in the 10 ft x 10 ft Supersonic Wind Tunnel at the NASA Lewis Research Center. For the first time, a solution is obtained for this configuration with the actual geometry, the tunnel conditions, and all the bleed zones modelled in the computation. Pitot pressure profiles and static pressures at various locations in the inlet are compared with the corresponding experimental data. The effect of bleed zones, located in different places on the inlet walls, in eliminating the low energy vortical flow generated from the 3-D shock-boundary layer interaction is simulated very well even though some approximations are used in applying the bleed boundary conditions and in the turbulence model. A further detailed study of the effect of individual bleed ports is needed to understand fully the actual mechanism of efficiently eliminating the vortical flow from the inlet. A better turbulence model would help to improve the accuracy even further in predicting the corner flow boundary layer profiles.

Introduction

The flow through a typical hypersonic inlet is characterized by complex three dimensional phenomena such as strong secondary flows and shock-boundary layer interactions. Since these phenomena can have significant effects on the overall performance of the inlet, any numerical method used to simulate the flow through the inlet must be capable of accurately predicting these complex phenomena. Therefore it is essential that the code selected for computing the inlet flows be thoroughly validated with experimental data to verify the code's capability to correctly simulate the flow features mentioned above. The object of this study is to validate the numerical code, selected for inlet flow computations, using the data obtained from an experimental study of a Mach 5 inlet conducted here at NASA Lewis Research Center's 10 x 10 ft. Supersonic Wind Tunnel facility.

A time marching full Navier-Stokes code, PARC3D,[1] was selected for the inlet flow computations. The PARC3D code solves the full three dimensional Reynolds averaged Navier-Stokes equations in strong conservation form with the Beam and Warming approximate factorization. The code was originally developed as AIR3D by Pulliam and Steger,[2] and Pulliam[3] later added the Jameson[4] artificial dissipation and called the code ARC3D. Cooper[1] adapted the code for internal flow in propulsion applications and named the code PARC3D. The PARC3D code uses central differencing on a generalized curvilinear coordinate system with implicit and explicit second and fourth order artificial dissipation. To simplify the solution of the block pentadiagonal system of discretized equations, the block implicit operators are diagonalized by decomposing the flux Jacobians, resulting in a scalar pentadiagonal

* Supervisor, Turbomachinery Analysis Section, Member AIAA
** Deputy Chief, Computational Methods Branch
*** Aerospace Engineer, Member AIAA

system. The loss of time accuracy from the diagonalization does not affect the spatial accuracy of the steady state solution.[3] The turbulence model used in the code for this study is the Baldwin-Lomax model.

The PARC3D code has been verified previously for 3-D supersonic and 2-D hypersonic flow configurations[5] with flow features similar to those of hypersonic inlets. These studies demonstrated the capability of PARC3D to simulate the hypersonic inlet flow phenomena. There was an attempt to compute the flow through a hypersonic inlet model (Generic Option 2 Mach 12.25 model[6]) which was experimentally tested by McDonnell-Douglas at the Calspan test facility. However, the experimental data indicated a turbulent transition in the corner regions of the inlet, the bulk of the flow through the inlet being laminar. Since the turbulence model in the code does not have the capability to simulate this three dimensional transition, a complete code validation could not be done with the available data. In the present experimental setup, the incoming flow was tripped by means of a grit to make the flow completely turbulent before it entered the inlet and it remained turbulent through the entire inlet.

The Mach 5 inlet configuration has been previously analyzed by Benson,[7] and by Kim et. al. [8] using a Parabolized Navier-Stokes (PNS) method, and by Rose[9] using the MacCormack algorithm. However, none of these computations simulated the actual experimental configuration in terms of the flow conditions and the inlet geometry. Benson's computations did not contain any bleed and the inlet Mach number was assumed to be 5.0, whereas the actual inlet has extensive bleed regions on the side walls as well as on the ramp and cowl surfaces. In addition, the Mach number of the flow at the entrance to the inlet in the wind tunnel was 3.5 with the inlet set up at a negative angle of attack of 8.5 degrees so that the flow goes through an expansion at the entrance to a Mach number of 4.1. This value is approximately equal to that corresponding to a flight Mach number of 5 with a 9 degrees angle of attack. Kim also assumed an entrance Mach number of 5 and computed the flow with only ramp and cowl bleed. Rose's configuration used side walls beginning from the first ramp instead of full side walls extending all the way to the leading edge of the precompression ramp (see Fig. 1). Moreover, only the corner bleed was considered in his computations.

In the present study all the bleed regions, fixed and variable, are simulated in the computation with the actual flow conditions and the geometry used in the wind tunnel.

Experimental Configuration

The experimental inlet is a scaled down model (1/3 scale) of a proposed Mach 5 aircraft mixed-compression inlet (the configuration is shown in Fig. 1). Since the maximum Mach number that can be obtained in the 10 x 10 Supersonic Wind Tunnel at NASA Lewis is 3.5, the inlet is set up at a negative angle of attack of 8.5 degrees so that the flow entering the inlet goes through an expansion on the precompression ramp to a Mach number of about 4.1. This setup is approximately equivalent to that of a flight Mach number of 5.0 at a 9 degrees angle of attack. The Mach number of the flow entering the inlet in the experiment was 3.49 and the tunnel total pressure was 35.1 psi. The Reynolds number based on the tunnel conditions with the cowl height (16 in), which is also equal to the width of the inlet, as the reference length was 3.3 million. A series of wedges (ramps) generate oblique shock waves external to the cowl. The cowl generates an oblique shock inside the inlet, which reflects from the ramp surface and terminates in a normal shock downstream of the inlet throat. A subsonic diffuser compresses the flow further and takes it to the exit duct. The computations in this study are performed to model only the supersonic portion of the flow through the inlet which includes the throat region upstream of the terminal normal shock.

To control shock-boundary layer interaction through the inlet, boundary layer bleed is provided on the inlet walls. A number of fixed and variable bleeds are set up in the throat region to obtain data with various bleed combinations. The original purpose of the test was to determine the minimum amount of bleed needed to keep the inlet started. The data obtained includes static pressures and pitot pressure distributions on the ramp, cowl, and side wall surfaces and in the corner regions at various axial locations through the inlet. Complete details of the experimental set up and the data can be found in reference 10.

Computations

The computations are performed on the Numerical Aerodynamic Simulation's Cray-2 computer, located at NASA Ames Research Center, using a grid size of 151 x 81 x 41. The computational grid showing one each of the stream wise and transverse planes is shown in Fig. 2. To resolve the viscous layers, the grid lines are clustered in regions close to the walls using hyperbolic tangent functions such that the first grid line away from the wall is located at a y^+ of approximately 2.0.

As shown in Fig. 2, the grid lines in the stream wise direction are arranged in such a way that the uppermost grid line follows the edge of the side wall which joins the leading edge of the inlet ramp with the inlet cowl on each side of the inlet. This arrangement facilitates the application of boundary conditions along the edges of the side wall.

Since the inlet is symmetric in the transverse (Z) direction, only half of the inlet flow field is computed, with a symmetry condition imposed on the center plane. A nonreflective boundary condition, using a simple Mach wave extrapolation, is applied on the upper boundary upstream of the cowl to let the shock waves from the first and second ramps pass through the boundary. The flow field at the inflow boundary, which is ahead of the inlet ramp leading edge, is held fixed, while at the outflow boundary, the flow variables are extrapolated from inside. No-slip condition is applied on all of the solid walls.

Bleed is simulated in the computations by imposing a constant mass flow through the porous bleed surfaces. The mass flow through the individual bleed regions has been obtained from the experimental data. A more accurate method of modeling the bleed would be to compute the flow through the bleed surfaces by including the plenum and the exit tube of each of the bleeds in the computational domain. However, including these regions in the 3-D computations would enormously increase the complexity of the grid generation and the computational times. Therefore, imposing the experimentally measured mass flow through the bleed surfaces and treating them as computational boundaries is considered a practically feasible and yet reasonably accurate way of simulating the bleed in the present study. It should be noted that these are the first calculations that modeled the actual test conditions, geometry, and bleed configuration.

Results and Discussion

An initial solution was obtained with no bleed on any of the inlet surfaces, although the inlet had unstarted in the wind tunnel with all the bleeds shut off. A close examination of the solution showed a separation bubble near the throat region, which kept growing slowly with increasing number of iterations. If the computation was continued in a time-consistent manner, the nature of the solution indicated that the inlet would unstart. However, the solution thus obtained could still be compared with the experimental data in the region upstream of the throat since the bleed does not affect the predominantly supersonic flow there so long as the solution had not shown the actual unstart. Hence the comparison of this initial solution, obtained with no bleed, with the experimental data upstream of the throat was presented in reference 10. The data included only a couple of pitot pressure rakes and static pressure distributions along the ramp and cowl center lines up to the throat.

The present computations are performed with the bleed boundary conditions applied on the surfaces corresponding to the various bleed zones. The solution is obtained for flow conditions identical to those of the experiment with all the bleed ports open. A schematic of the bleed regions, denoted by shaded surfaces, along with the outline of the duct geometry, is shown in Fig. 3.

Fig. 4 shows the Mach number contours in the cross planes at selected axial locations. The figure shows shock waves from the different ramp surfaces and the cowl as horizontal lines, and the interaction of the shocks with the boundary layer on the side walls. The strong secondary flow set up by this shock-boundary layer interaction and the migration of the low energy fluid towards the center plane of the inlet as the flow approaches the throat can be clearly seen in Fig. 4. It is the presence of this low energy fluid occupying a significant portion of the inlet cross sectional area that degrades the performance of the inlet. The purpose of the bleeds is to remove this low energy fluid from the inlet and thereby improve the total pressure recovery. As the flow approaches the throat region that contains bleed, the undesirable low energy fluid is reduced considerably (see Fig. 4). This phenomenon has been substantiated by the experimental data of the two corner rakes which will be discussed in the later portion of this section.

By examining the location of various bleed ports, shown in Fig. 3, it can be seen that a combination of the first cowl bleed, the side wall bleed underneath the first cowl bleed, and the downstream cowl bleed appears to be responsible for the elimination of the low energy vortical fluid. This region is shown in more detail in the pitot pressure contours along with the bleed zones in Fig. 15b, which is discussed in a later portion of this section. A systematic study involving different computational runs with selected bleed zones open would help in understanding which of these bleed zones has a major influence in eliminating the low energy fluid. Additional computations are planned to study this phenomenon in more detail. This study will be coordinated

with the second entry experiments planned to be run in the 10 ft x 10 ft Supersonic Wind Tunnel at NASA Lewis in the near future.

It should be pointed out here that previous calculations by Rose[9] have indicated that the corner bleed regions do not remove the vortical flow from the inlet. It can be seen from Figs. 3 and 4 that the side wall bleed located upstream of the cowl seems to have little effect in eliminating this low energy fluid. This fact has also been observed in experiments by Barnhart[11] and computations by Gaitonde[12] of glancing shock-side wall boundary layer interactions. It could be argued that the downstream throat bleed would not have a major influence on the predominantly supersonic flow in the corner region. However, as mentioned earlier, further calculations isolating different bleed regions are needed either to confirm or disprove these arguments.

Static pressures on the ramp surface both along the centerline and 7.5 inches from the center line are compared to the corresponding experimental data in Fig. 5. The static pressures and the pitot pressures in all of the comparisons are nondimensionalized with the tunnel static pressure (0.467 psi); the lengths are normalized with cowl height (16 in.). The agreement of the solution with the data is very good throughout the computational length of the inlet. Fig. 6 shows a similar comparison for the cowl surface; once again the agreement between the data and the solution is good except in the initial portion where the disagreement is with three of the data points on the center line and one point at 7.5 inches from the center line. It has been found that one of the translating probe assemblies is located in the same region where these four static pressure taps are located. The probe assemblies used in the experiment do not completely retract into the walls of the inlet; instead they project about 1/8 inch into the flow. Because shock waves are generated from this projection, the data obtained from these four static pressure taps, where the solution disagrees with the data, are not accurate.

Pitot pressure profiles are compared at various locations on the ramp, cowl, and side wall surfaces. To determine the ability of the bleed ports to bleed the low energy vortical fluid out of the inlet, two rakes are mounted in the corner of the cowl and the side wall surface at a 45 degrees angle in the throat region. A number of translating probes were also used to measure pitot pressure profiles at various locations on the ramp and side wall surfaces. Since it is not possible to present the comparison of the solution with the data from all of the rakes and probes, only a few rakes and probes, placed in each of the important regions of the inlet flow field, have been selected. The rake and probe numbers and their locations for which the solution was compared are shown in Fig. 7.

Figures 8-12 compare the solution with the experimental data corresponding to pitot pressure rakes located on the ramp surface both along the center line and close to the side wall at various stream wise stations. These comparisons show that, in general, the agreement between the solution and the experimental data is very good along the center line (rakes 1, 3 and 6). Close to the side wall the agreement is not so good (rakes 2 and 7). This disagreement can be attributed to the corner effect that could not be adequately simulated with the present turbulence model. A better turbulence model is believed to improve the comparison in the corner regions.

Figures 13 and 14 show pitot pressure comparisons corresponding to rake 10 and 13. These rakes are mounted from the corner of the cowl and side wall surfaces at a 45 degrees angle to the surfaces. Rake 10 is located at 59.6 in. and rake 13 is located at 68.5 in. from the start of ramp 1 (see Figs. 1 and 7). As mentioned earlier, most of the low energy vortical flow is removed from the inlet between these two rakes. The profile of rake 10 shows great variations in the pitot pressure as we move along the rake away from the corner.

This variation in the pitot pressure due to the presence of the vortical flow can also be seen in the pitot pressure contours in Figs. 15a and 15b. Fig. 15a shows the pitot pressure contours for the two cross sections corresponding to rake 10 and rake 13, along with the rake locations in the cross sections. Fig. 15b shows the pitot pressure contours for the two cross sections of rakes 10 and 13, as well as a third location in between. Also shown in Fig. 15b as shaded surfaces are the various bleed zones in this region. Considering the location of the rake, the nature of the flow, and the approximation used in the turbulence model, the agreement between the solution and the experimental data is reasonably good. The pitot pressure profile for rake 13, shown in Fig. 14, does not show the variation of rake 10 except for a small bump very close to the corner. The pitot pressure contours for the cross section corresponding to rake 13, shown in Fig. 15, reveal that most of the vortical flow has been removed before it reached this stream wise location. Once again the agreement between the solution and the experimental

data, corresponding to rake 13, is good.

Figures 16-20 show pitot pressure profile comparisons for the translating probes located at different stream wise stations on the ramp as well as on the side wall surfaces. Considering that these probes are located in a very complex part of the flow, the agreement is good between the solution and the experimental data for the locations away from the corner regions (probes 9 and 11). The slight disagreement in the corner regions (probes 2, 5, and 10) is, as mentioned earlier, believed to be due to the approximations used in the turbulence model.

Summary

A 3-D viscous solution has been obtained for an experimental Mach 5 inlet configuration in order to validate the PARC3D code for hypersonic inlet applications. The flow has been computed with bleed on the inlet walls identical to that used in the experiment. These are the first computations for this configuration obtained with the actual geometry, flow conditions, and the bleeds identical to those of the experiment. Comparison between the solution and the experimental data indicates that the PARC3D code is fully capable of predicting the strong secondary flows and the 3-D shock-boundary layer interaction typically present in the hypersonic inlets.

The PARC3D code also appears to correctly indicate that the inlet would unstart if there was no bleed on the inlet walls. The mechanism of bleeding the undesirable vortical flow to improve the performance of the inlet has been simulated very well by the code. With a better understanding of the actual process which removed most of the vortical flow when the bleed region is actually below the vortical structure, the code could be used in the inlet design procedure to optimize the bleed port locations to remove the low energy fluid efficiently and improve the inlet total pressure recovery.

Acknowledgement

This research is supported by NASA Lewis Research Center under contract NAS3-25266 with Thomas J. Benson as monitor.

References

1. Cooper, G.K., Jordan, J.L., and Phares, W.J., "Analysis Tool for Application to Ground Testing of Highly Underexpanded Nozzles", AIAA 87-2015, 1987.

2. Pulliam, T.H., and Steger, J.L., "Implicit Finite-Difference Simulations of Three Dimensional Compressible Flow.", AIAA Journal, Vol. 18, February 1980, pp. 159-167.

3. Pulliam, T.H., "Euler and Thin Layer Navier-Stokes Codes: ARC2D, ARC3D", Notes for Computational Fluid Dynamics User's Workshop, The University of Tennessee Space Institute, Tullahoma, Tennessee, March 12-16, 1984.

4. Jameson, A., Schmidt, W. and Turkel, E., "Numerical Solutions of the Euler Equations by Finite Volume Method Using Runge-Kutta Time Stepping Schemes", AIAA 81-1259, 1981.

5. Reddy, D.R., and Harloff, G.J., "Three Dimensional Viscous Flow Computations and High Area Ratio Nozzles for Hypersonic Propulsion", AIAA paper 88-0474, January, 1988.

6. Reddy, D. R., Smith, G. E., Liou, M.-F., and Benson, T. J., "Three Dimensional Viscous Analysis of a Hypersonic Inlet," AIAA Paper 89-0004, January 1989.

7. Benson, T. J., "Three Dimensional Viscous Calculation of Flow in a Mach 5 Hypersonic Inlet," AIAA Paper 86-1461, June 1986.

8. Kim, Y. N., Buggelin, R. C., and McDonald, H., "Numerical Analysis of Some Supersonic Viscous Flows Related to Inlet and Nozzle Systems," AIAA Paper 86-1597, June 1986.

9. Rose, W. C., and Perkins, E. W., "Innovative Boundary Layer Control Methods in High Speed Inlet System," Final Report, Phase I, SBIR Contract No. NAS3-25408, NASA Lewis Research Center, September 1988.

10. Weir, L. J., Reddy, D. R., Rupp, G. D., "Mach 5 Inlet CFD and Experimental Results," AIAA paper 89-2355, July 1989.

11. Barnhart, P.J., Greber, I., and Hingst, W. R., "Glancing Shock Wave-Turbulent Boundary Layer Interaction with Boundary Layer Suction," AIAA Paper 88-0308, January 1988.

12. Gaitonde, D., and Knight, D., "The Effect of Bleed on the Flowfield Structure of the 3-D Shock Wave-Boundary Layer Interaction Generated by a Sharp Fin," AIAA Paper 88-0309, January 1988.

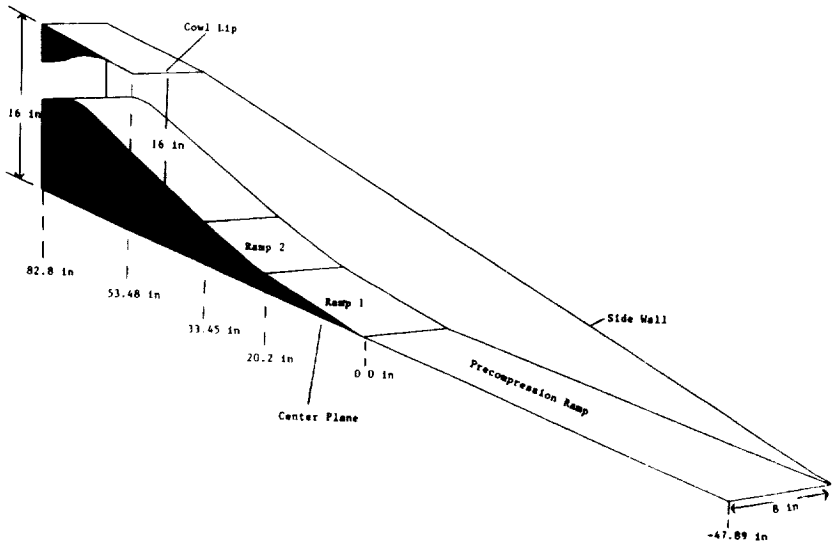

Figure 1. Inlet Model Configuration

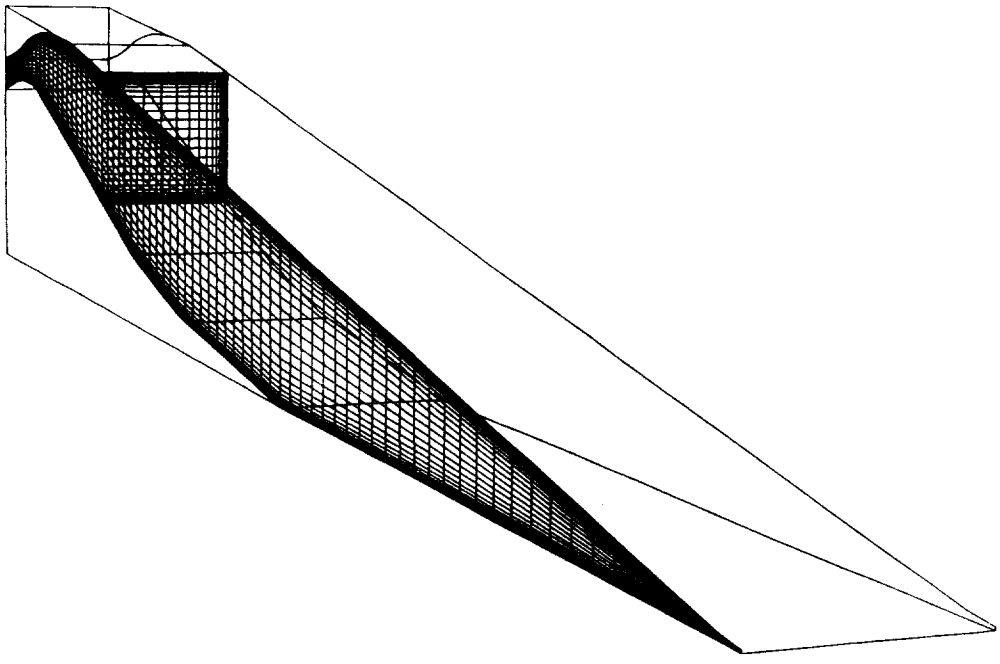

Figure 2. Computational Grid

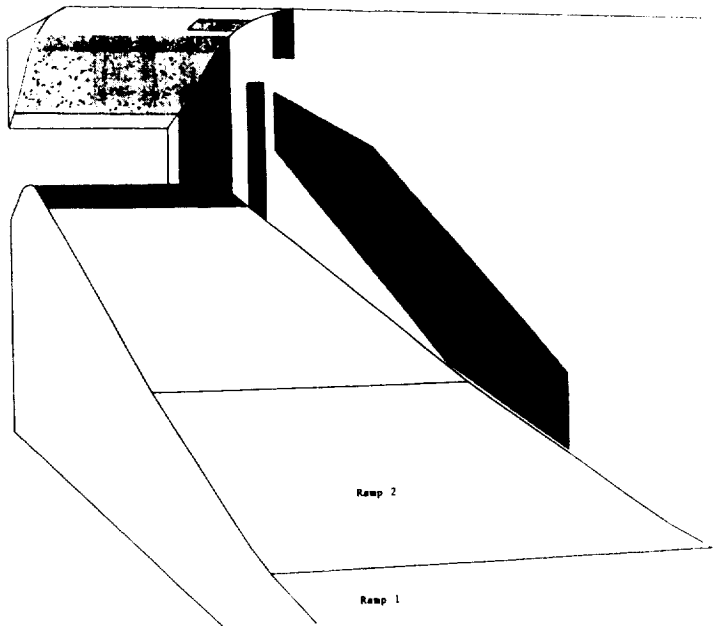

Figure 3. Bleed Zones

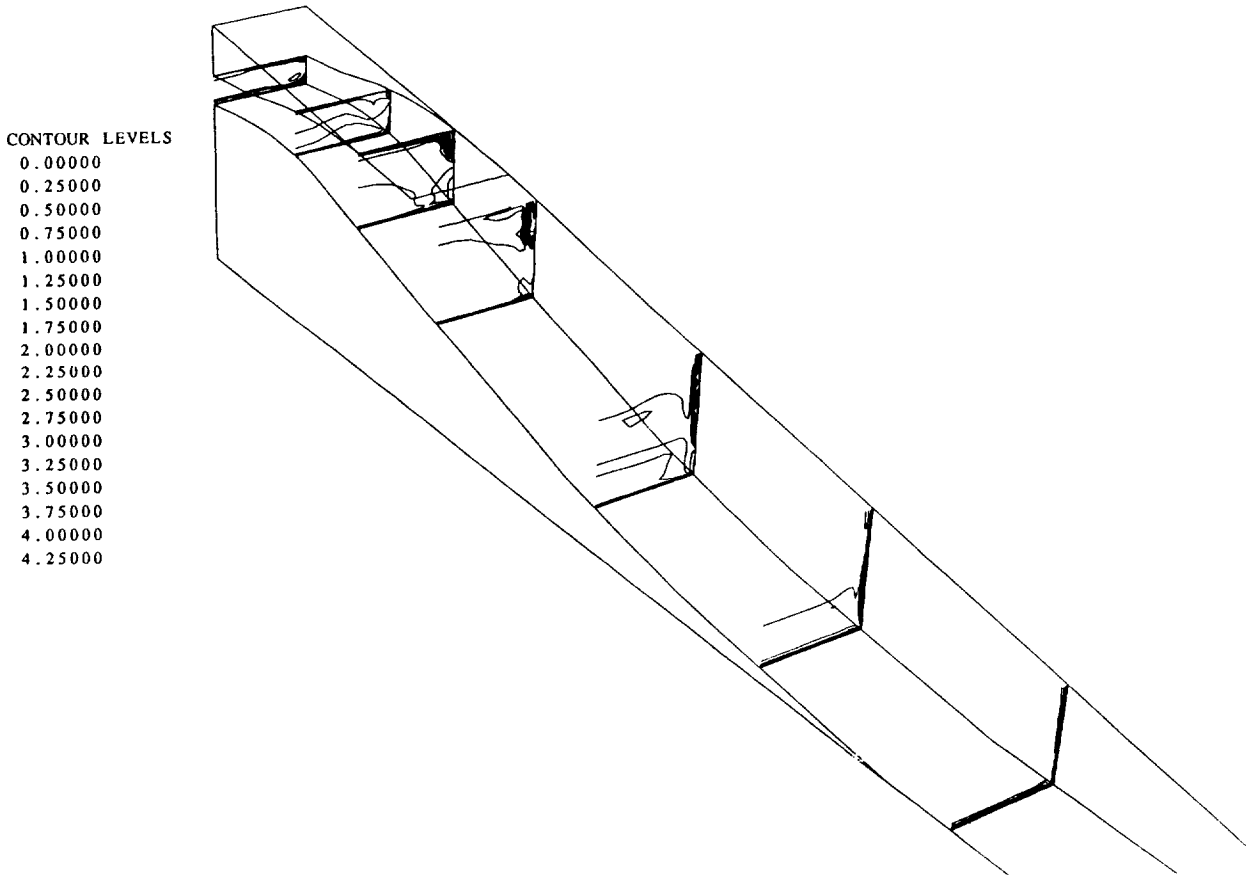

Figure 4. Mach Number Contours

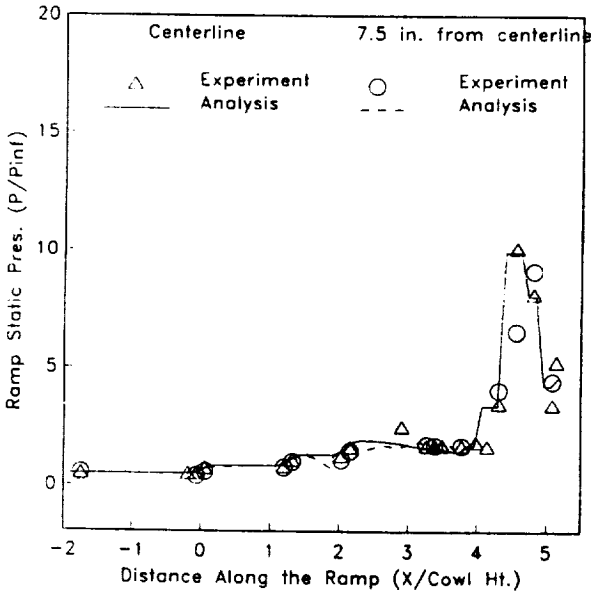

Figure 5. Ramp Static Pressure Distribution

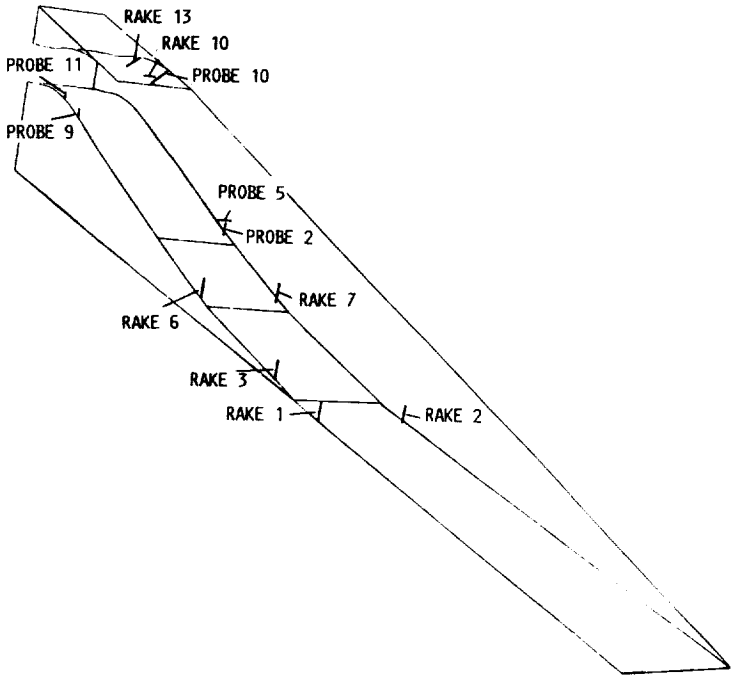

Figure 7. Location of Fixed Rakes and Translating Probes Used for Pilot Pressure Measurement

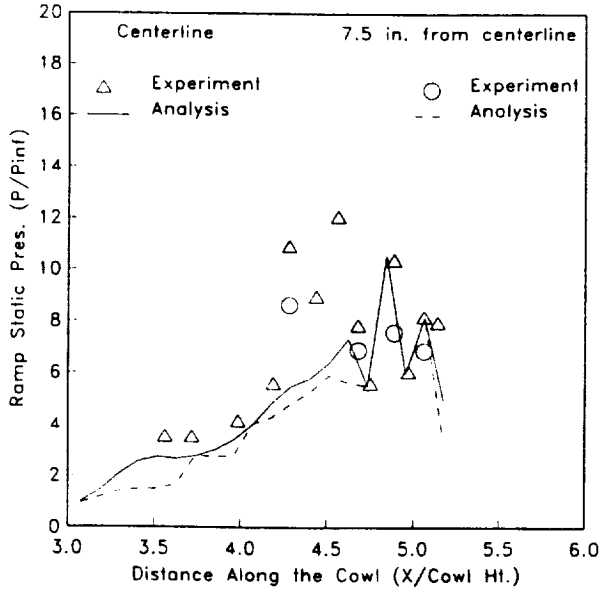

Figure 6. Cowl Static Pressure Distribution

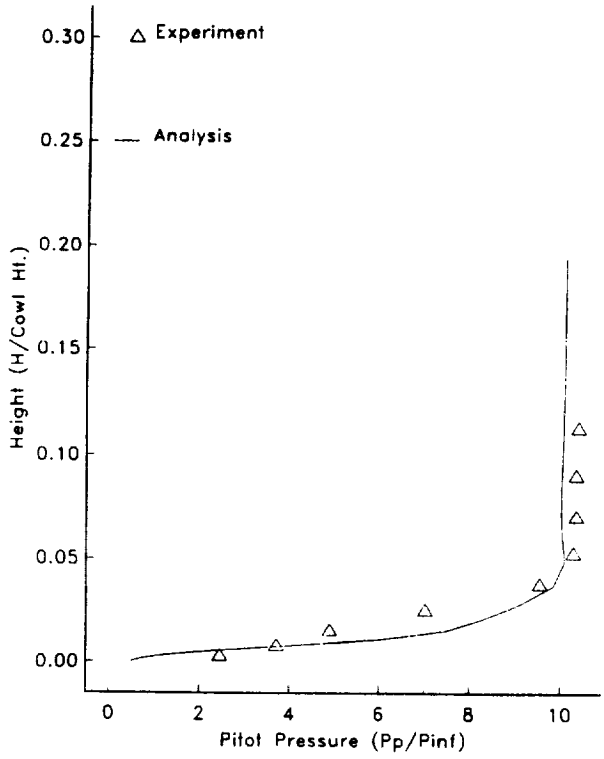

Figure 8. Rake 1 Pitot Pressure Profile

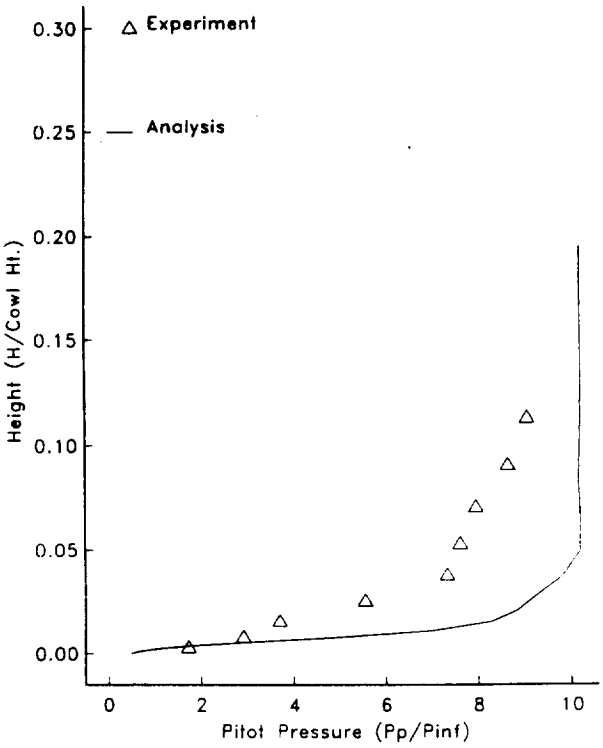

Figure 9. Rake 2 Pitot Pressure Profile

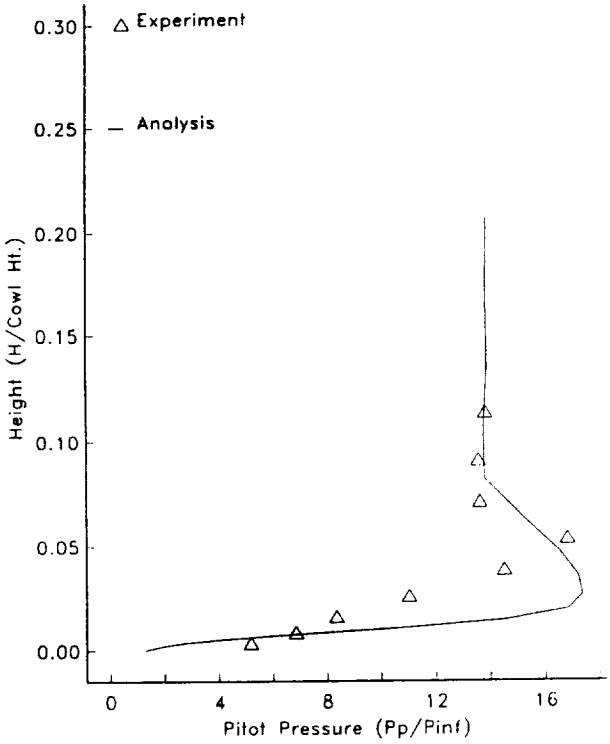

Figure 11. Rake 6 Pitot Pressure Profile

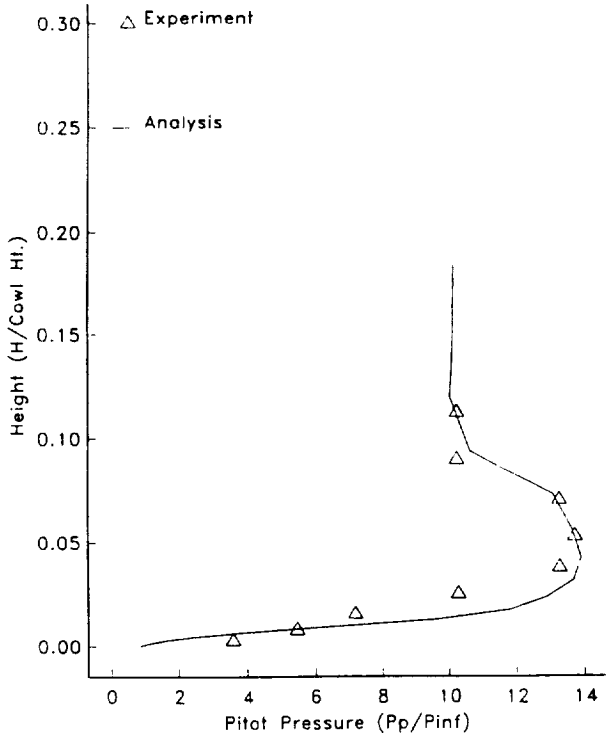

Figure 10. Rake 3 Pitot Pressure Profile

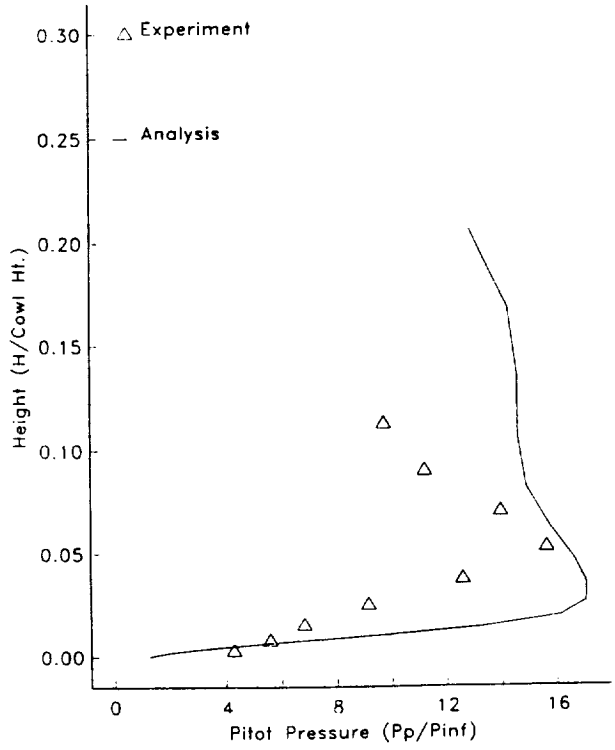

Figure 12. Rake 7 Pitot Pressure Profile

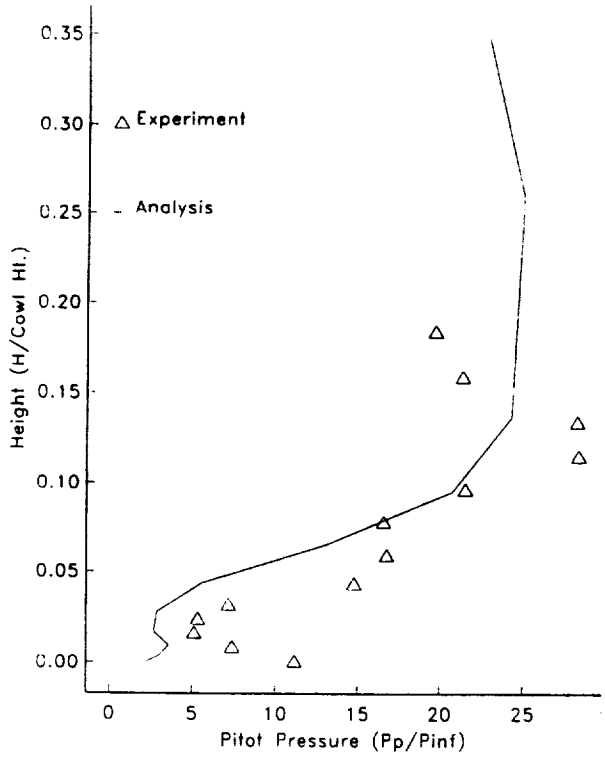

Figure 13. Rake 10 Pitot Pressure Profile

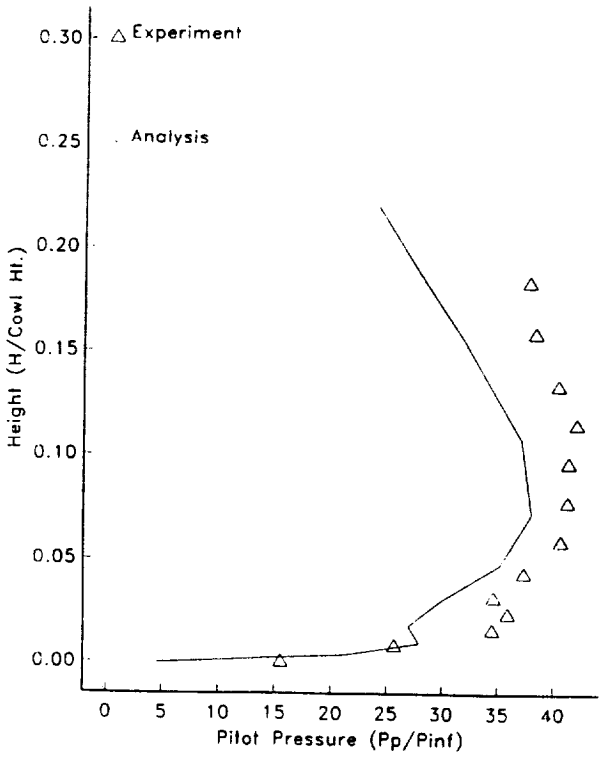

Figure 14. Rake 13 Pitot Pressure Profile

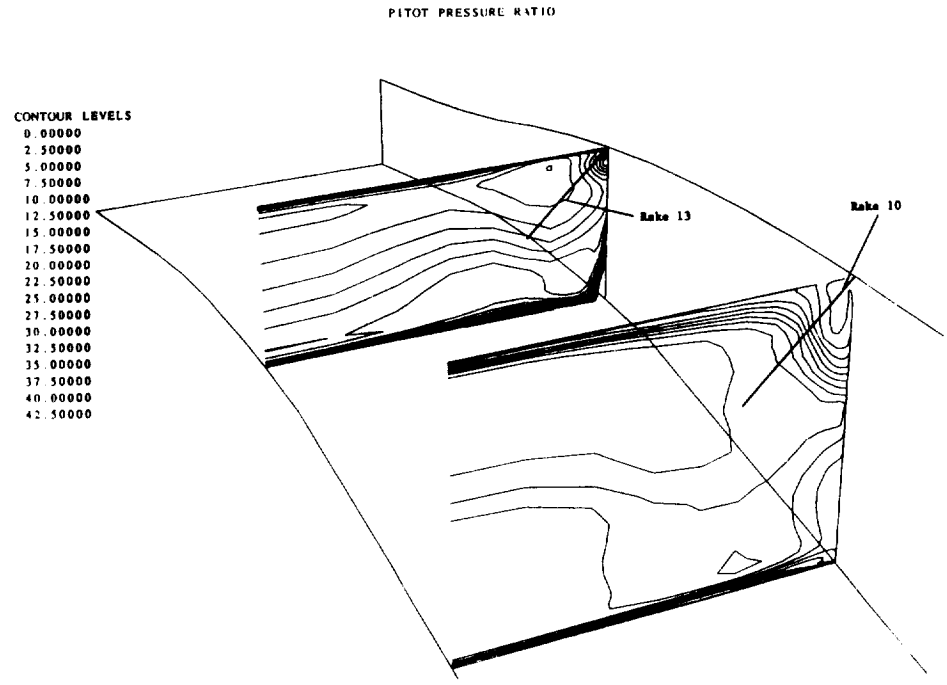

Figure 15a. Pilot Pressure Contour at Rake 10 and Rake 13

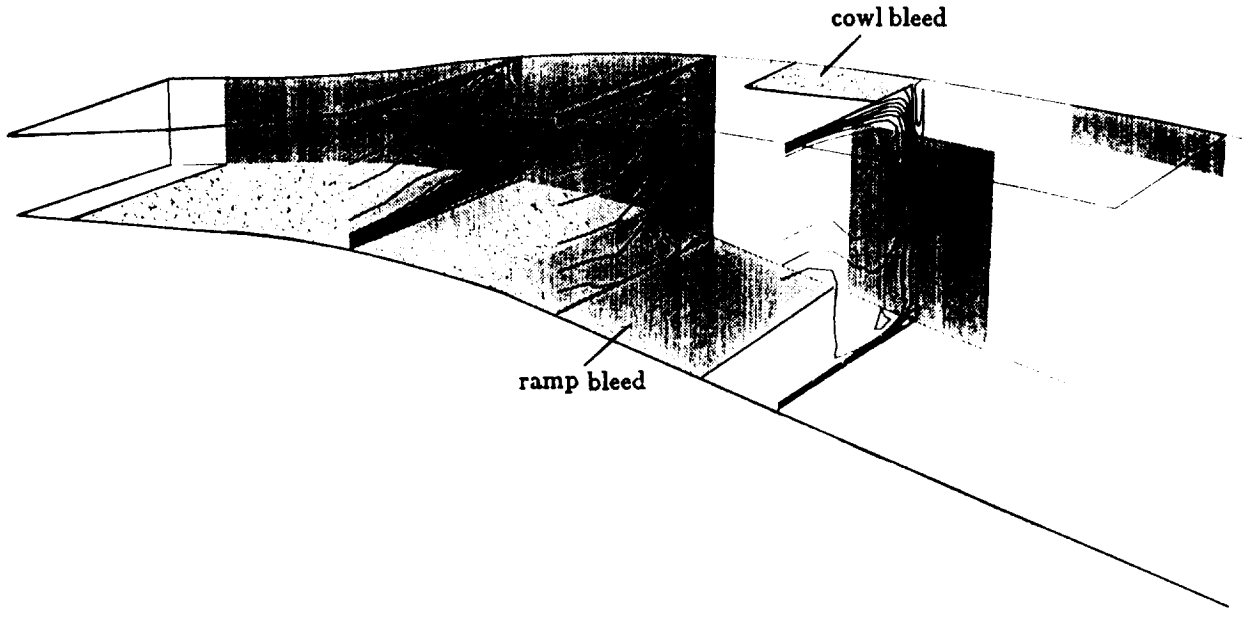

Figure 15b. Pilot Pressure Contours Between Rake 10 and Rake 13 and Bleed Zones

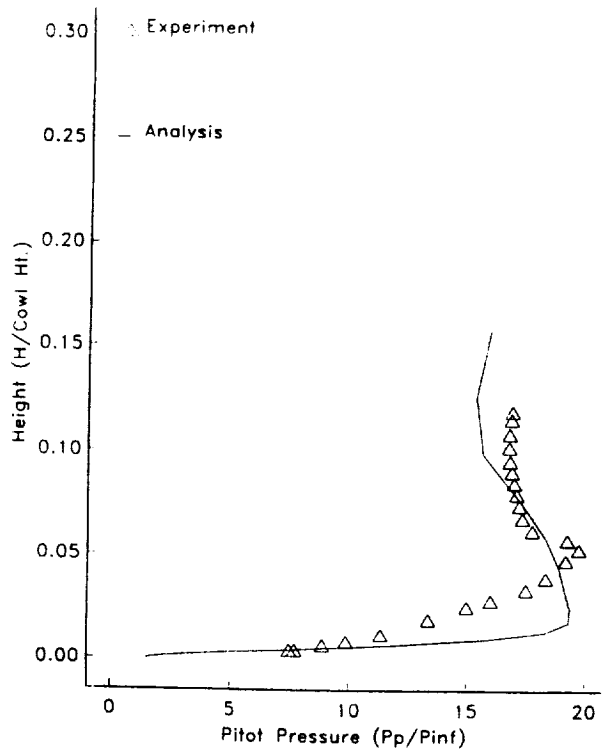

Figure 16. Probe 2 Pitot Pressure Profile

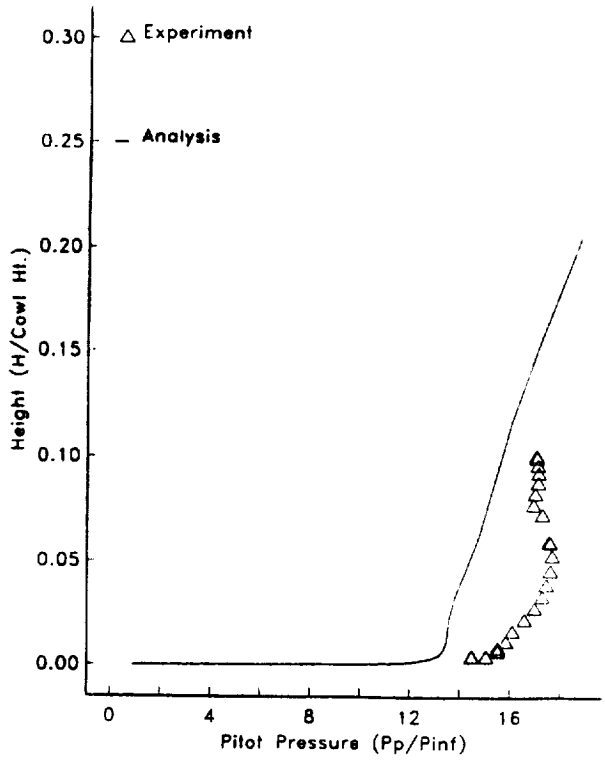

Figure 17. Probe 5 Pitot Pressure Profile

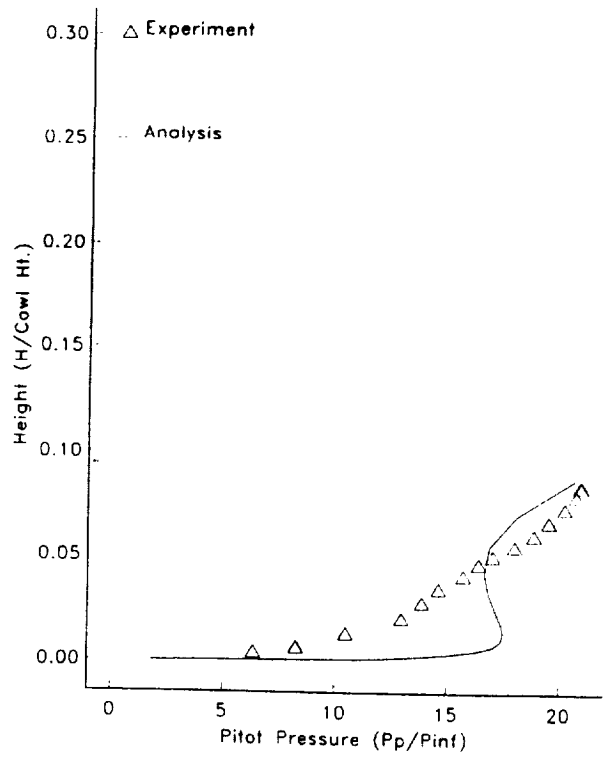

Figure 18. Probe 9 Pitot Pressure Profile

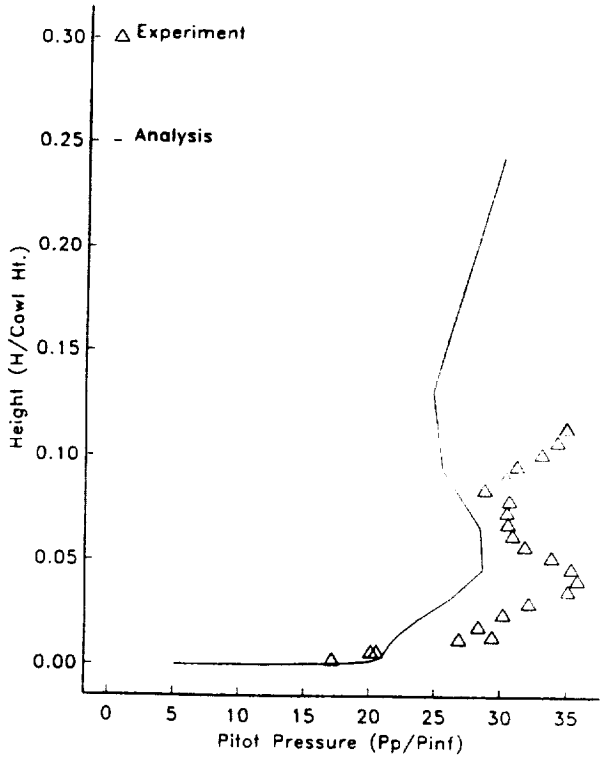

Figure 19. Probe 10 Pitot Pressure Profile

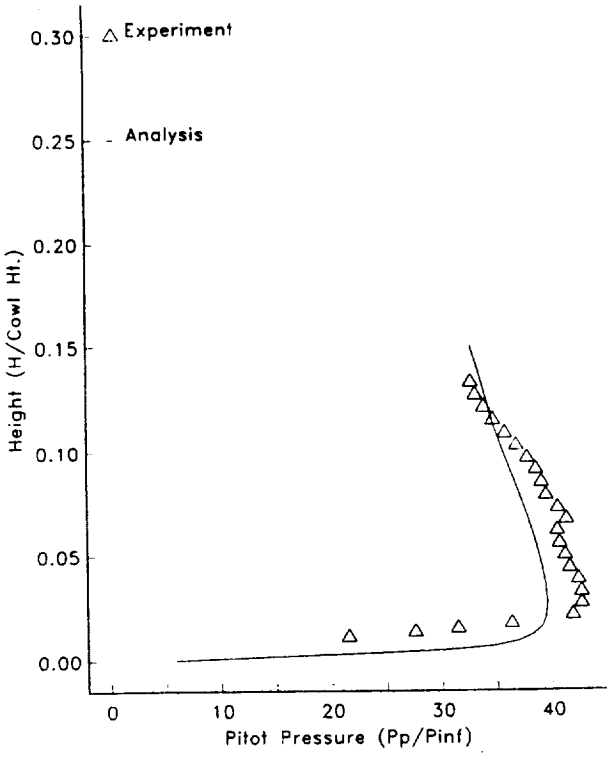

Figure 20. Probe 11 Pitot Pressure Profile

NASA
National Aeronautics and Space Administration

Report Documentation Page

1. Report No.	2. Government Accession No.	3. Recipient's Catalog No.
NASA TM-102518 AIAA-90-0600		

4. Title and Subtitle

Comparison of 3-D Viscous Flow Computations of Mach 5 Inlet With Experimental Data

5. Report Date

6. Performing Organization Code

7. Author(s)

D.R. Reddy, T.J. Benson, and L.J. Weir

8. Performing Organization Report No.

E-5322

10. Work Unit No.

505-62-21

9. Performing Organization Name and Address

National Aeronautics and Space Administration
Lewis Research Center
Cleveland, Ohio 44135-3191

11. Contract or Grant No.

13. Type of Report and Period Covered

Technical Memorandum

12. Sponsoring Agency Name and Address

National Aeronautics and Space Administration
Washington, D.C. 20546-0001

14. Sponsoring Agency Code

15. Supplementary Notes

Prepared for the 28th Aerospace Sciences Meeting sponsored by the American Institute of Aeronautics and Astronautics, Reno, Nevada, January 8-11, 1990. D.R. Reddy, Sverdrup Technology, Inc., NASA Lewis Research Center Group, Cleveland, Ohio 44135. T.J. Benson and L.J. Weir, NASA Lewis Research Center.

16. Abstract

A time marching 3-D full Navier-Stokes code, called PARC3D, is validated for an experimental Mach 5 inlet configuration using the data obtained in the 10 ft × 10 ft Supersonic Wind Tunnel at the NASA Lewis Research Center. For the first time, a solution is obtained for this configuration with the actual geometry, the tunnel conditions, and all the bleed zones modelled in the computation. Pitot pressure profiles and static pressures at various locations in the inlet are compared with the corresponding experimental data. The effect of bleed zones, located in different places on the inlet walls, in eliminating the low energy vortical flow generated from the 3-D shock-boundary layer interaction is simulated very well even though some approximations are used in applying the bleed boundary conditions and in the turbulence model. A further detailed study of the effect of individual bleed ports is needed to understand fully the actual mechanism of efficiently elminating the vortical flow from the inlet. A better turbulence model would help to improve the accuracy even further in predicting the corner flow boundary layer profiles.

17. Key Words (Suggested by Author(s))	18. Distribution Statement
3-D turbulent full Navier-Stokes computations Hypersonic inlet Code validation	Unclassified – Unlimited Subject Category 07

19. Security Classif. (of this report)	20. Security Classif. (of this page)	21. No. of pages	22. Price*
Unclassified	Unclassified	14	A03

NASA FORM 1626 OCT 86

*For sale by the National Technical Information Service, Springfield, Virginia 22161